Estimating the principal dynamic modes of autonomic state with wearable sensors

Jongyoon Choi and Ricardo Gutierrez-Osuna
Department of Computer Science, Texas A&M University, College Station, TX 77843
{goonyong, rgutier}@cs.tamu.edu

Abstract

The relationship between the autonomic nervous system and the heart provides a window into our internal state, e.g., stressed vs. relaxed. This relationship has received extensive attention in cardiovascular physiology, typically with electrocardiogram recordings under laboratory conditions (e.g., pharmacological blockade). This article presents a signal-processing method to estimate autonomic activation using heart-rate monitors under more naturalistic conditions. The method uses non-linear system identification and eigen-analysis to decouple contributions from the two autonomic branches (i.e., sympathetic and parasympathetic). We validate the method using experimental data from a wearable sensor platform that we have designed for experience sampling. Using a discrimination test between two physiological conditions (supine and tilt), we show that our method outperforms traditional techniques based on spectral analysis of heart rate variability.

1. Introduction

We engage in regular activities every day; we commute to work at regular times, run errands at specific locations, and interact with a stable group of individuals. Life consists of a series of these experiences, some of which can affect our health and our mood. Being able to log our internal states in relation to these behaviors and surroundings may allow us to unveil "life patterns" and develop insights about them. However, it is impractical to annotate painstakingly what we do and how we feel during the day. In some cases, we may not even be aware of our own physiological changes to a contextual stimulus. For this purpose, we are developing a minimally obtrusive wearable sensor platform that can capture a variety of context and physiological signals. This article describes the first step of the process: estimating autonomic state.

The autonomic nervous system (ANS) is responsible for maintaining and controlling the involuntary effectors of the body, such as contraction of smooth muscles in organs (e.g. blood vessels, eyes, lungs, bladder, gastrointestinal tract) and regulation of the heart and glands [1]. The ANS is composed of two main branches: the sympathetic nervous system (SNS) and the parasympathetic nervous system (PNS); the latter is also known as the vagal branch. The SNS responds to impending danger or stress, and is responsible for increasing one's heartbeat and blood pressure. The PNS promotes calming of the nerves to return to regular function, and is evident when a person is resting and feels relaxed. Thus, SNS and PNS activity can provide an indirect measure of psychological state [1].

2. Physiological background

Both autonomic branches innervate the sinoatrial node, the primary pacemaker site in the heart; SNS activation increases heart rate, whereas PNS activation reduces it. This suggests that heart rate can be used to estimate the activation level of both autonomic branches and, indirectly, predict psychological state. Unfortunately, changes in SNS versus PNS activity are potentially indistinguishable based only on changes in heart rate, e.g., an increase of heart rate could be the result of increased SNS input and/or decreased PNS input. Instead, one must consider the dynamics of both branches: parasympathetic influences on heart rate take effect more rapidly. Thus, fluctuations in beat-to-beat periods provide information about the relative contribution of each branch. This is known as heart rate variability (HRV) analysis.

Frequency analysis of beat-to-beat time series shows three main spectral bands: very low-frequency (VLF; below 0.04 Hz), low-frequency (LF; between 0.04 and 0.15 Hz), and high-frequency (HF; between 0.15 and 0.5 Hz) [2]. The LF band reflects activity in both branches, whereas the HF band contains mainly PNS activity. As a result, the ratio of LF to HF power can serve as an index of autonomic balance[1]. Unfortunately, breathing patterns influence low-frequency and high-frequency power spectra [3], so the LF/HF ratio is only reliable under constant breathing rates. More importantly, LF/HF analysis is a linear

[1] The physiological underpinning of the VLF component is less clear. Moreover, VLF assessed from short-term recordings (i.e., less than 5 minutes) is a dubious measure and should be avoided.

method, whereas interactions between SNS and PNS branches are nonlinear [4, 5].

To address the limitations of conventional spectral analysis, this article presents a nonlinear system-identification technique for analyzing heart rate variability. Known as principal dynamic mode (PDM) analysis, the technique was originally developed by Marmarelis [6, 7] as a general method for modeling nonlinear biological systems. Recent results by Zhong et al. [4, 5] suggest that PDM can help decouple autonomic contributions to heart rate variability [4, 5]. In these studies, the authors relied on electrocardiogram (ECG) recordings and pharmacological blockade[2]. Their results showed that the two dominant dynamic modes correspond to SNS and PNS influences. Our work extends these studies in two respects that are particularly relevant to the wearable community. First, our approach focuses on consumer-grade heart-rate monitors rather than ECG monitors; this difference is important because heart-rate monitors are more economical (up to two orders of magnitude) and less cumbersome than ECG monitors. Second, our study does not rely on pharmacological blockade, and instead uses a naturalistic protocol based on body posture. In addition, we propose an alternative selection criterion to map the various dynamic modes into SNS or PNS contributions; this criterion is based on the polarity of the dynamic modes rather than their frequency content. Our results show that the PDM method provides better discrimination between physiological conditions than traditional power spectral analysis.

3. Wearable Platform

3.1. Design specifications

During the past year, we have developed a small wearable platform for experience sampling [8]. Our experimental needs called for a platform that could capture both physiological and contextual information. The system had to be open, to provide access to raw signals and full control of data-acquisition. The system had to be modular, to facilitate integration of additional sensors. The system had to be minimally obtrusive (e.g., no wires dangling around the user's body), lightweight, and relatively small. The system also had to be power-efficient, which we defined as continuous operation for at least 6 hours between battery charges. Finally, the system had to be low-cost (below $500). None of the commercial ambulatory systems available at the time satisfied all the above constraints, which prompted us to design a custom platform.

[2] In pharmacological blockade studies, subjects receive injections of propranolol and/or atropine, two drugs that suppress activity in the sympathetic and/or parasympathetic branches, respectively.

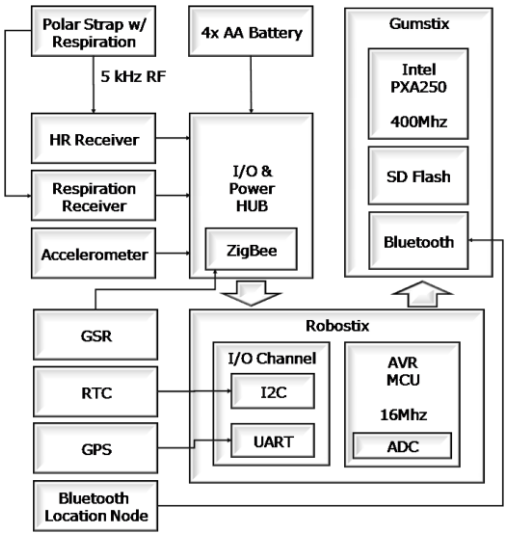

Figure 1. Architecture of the wearable device

3.2. Architecture

Our design is based on an embedded Linux-centric platform. The system consists of a Gumstix motherboard (Intel XScale® PXA255, 400 MHz, 64 MB RAM, xMB Flash; Gumstix, Inc.) and an add-on Robostix data-acquisition card. A Bluetooth port on the Gumstix and an additional ZigBee module allow us to interface wirelessly with multiple sensors. Figure 1 shows the configuration of the system and the sensors that are available. A sensor hub bridges the Robostix data-acquisition module with external sensors; the sensor hub is also responsible for supplying power to Gumstix, Robostix, and sensors. Raw sensor data is stored into a flash memory on the Gumstix, but it can also be streamed out to an external system for further analysis, remote storage, and real-time display. To date, we have integrated a 3D accelerometer (MMA7260Q; Freescale Semiconductor, Inc.), a GPS unit (EM-401A SiRF III Receiver; USGlobalSat, Inc.), a real time clock unit (DS1307; Dallas Semiconductor, Inc.), a heart rate transmitter (Polar T31; Polar Electro Inc.) and a custom-made respiration sensor. Figure 2 shows a picture of our prototype.

3.3. Physiological Sensors

Our initial choice of physiological measures has focused on heart and respiration signals. We measure heart signals with a heart rate monitor (HRM) that is very popular in the exercise-management area. This HRM detects R peaks in cardiac activity rather than the complete ECG signal, but is considerably less cumbersome (it requires no wiring) and is robust to physical activity. One potential issue with HRMs is whether the data is suitable for HRV analysis. To

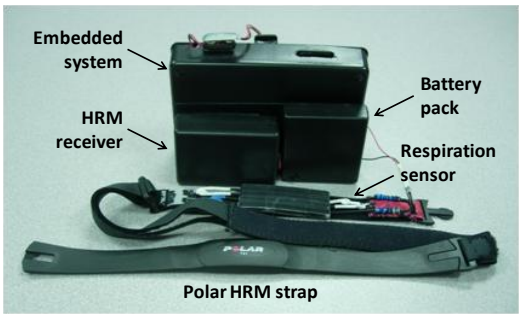

Figure 2. Hardware prototype of our experience sampling system

answer this question, Radespiel-Tröger et al. [9] performed a comparison between a Polar HRM and an ECG-based system. Their results showed good agreement between both devices in terms of heart rate, duration of R-R-intervals, and two standard time-domain measures of HRV.

The HRM transmitter generates a 5kHz electromagnetic pulse with each heart beat. We intercept this signal with a custom-built receiver circuit following a publicly-available design [10]. Finally, we sample the HRM signals at 500Hz, which falls within the recommendations of the 1996 Task Force report on HRV protocols [2].

We measure respiration with a custom-made sensor integrated into the HRM chest strap (see Figure 2). The sensor consists of a flexible cylindrical tube (∅ 0.06 in.) whose resistance increases with elongation. Respiration signals are sampled at 30 Hz. The respiration sensor is currently wired to the sensor hub, but a wireless ZigBee port is under development.

4. Nonlinear System Identification

Our autonomic-activity estimator is based on the principal dynamic mode (PDM) method of Marmarelis [6, 7]. The method employs a Volterra-Wiener series to model the nonlinear dynamics of the system, and an eigenvalue decomposition to extract the most significant dynamical components. A brief description of the PDM method follows; further details on kernel estimation are available in the appendix.

Assume a stable (finite-memory) nonlinear time-invariant dynamic system. Such system can be modeled with a discrete-time Volterra series as:

$$y(t) = k_0 + \sum_{\tau=0}^{M-1} k_1(\tau)x(t-\tau) + \sum_{\tau_1=0}^{M-1}\sum_{\tau_2=0}^{M-1} k_2(\tau_1,\tau_2)x(t-\tau_1)x(t-\tau_2) + \cdots \quad (1)$$

where $y(t)$ is the system's output , $x(t-\tau)$ is the system's input with a delay of τ, M is the memory of the model, and $(k_0, k_1, k_2, \dots)$ are the Volterra kernels, which describe the dynamics of the system. When modeling physiological systems, second-order series are commonly used to provide a balance between computational efficiency and expression power [6]. Using matrix notation, a second-order Volterra series becomes:

$$y(t) = X^T(t)QX(t)$$
$$where\ X(t) = \begin{bmatrix} 1 \\ x(t) \\ \vdots \\ x(t-M+1) \end{bmatrix} and\ Q = \begin{bmatrix} k_0 & \frac{1}{2}{k_1}^T \\ \frac{1}{2}k_1 & k_2 \end{bmatrix} \quad (2)$$

Since Q is symmetric, there always exists an orthonormal matrix R such that $Q = R^T \Lambda R$, where Λ is a diagonal eigenvalue matrix. This leads to:

$$y(t) = X^T R^T \Lambda R X = U^T \Lambda U = \sum_{i=0}^{M-1} \lambda_i u_i^2(t) \quad (3)$$

Thus, the output of the system $y(t)$ can be expressed as a weighted sum of functions $u_i^2(t)$. The *ith* principal dynamic mode (pdm_i) is then defined as the eigenvector[3] of Q that corresponds to the largest *ith* eigenvalue λ_i:

$$pdm_i = [\mu_{i,1} \quad \mu_{i,2} \quad \dots \quad \mu_{i,M}] \quad (4)$$

and the function $u_i(t)$ can be computed as the convolution of the tapped-delay input $X(t)$ with pdm_i:

$$u_i^2(t) = \{pdm_i * X(t) + \mu_{i,0}\}^2$$
$$where\ X(t) = [x(t) \quad \dots \quad x(t-M+1)] \quad (5)$$

By selecting the most significant eigenvalues from Λ, $y(t)$ can then be approximated with a small number of components:

$$\hat{y}(t) = \sum_{i=0}^{S} \lambda_i \{pdm_i * X(t) + \mu_{i,0}\}^2 \quad (6)$$

4.1. Generating an input signal

The PDM method assumes that both input $x(t)$ and output $y(t)$ are available. In our case, however, only an output signal is available: the heart rate (R-R) time series. To address this issue, we employ a similar strategy as Zhong et al. [4]. Namely, we assume that the input is a delayed and transformed version of the output: $x'(t) \sim f(y(t-1))$. Ideally, this input would be broadband and related to the output [7]. To achieve these characteristics, we first use the delayed output

[3] The first eigenvector is generally discarded, since it corresponds to a constant offset.

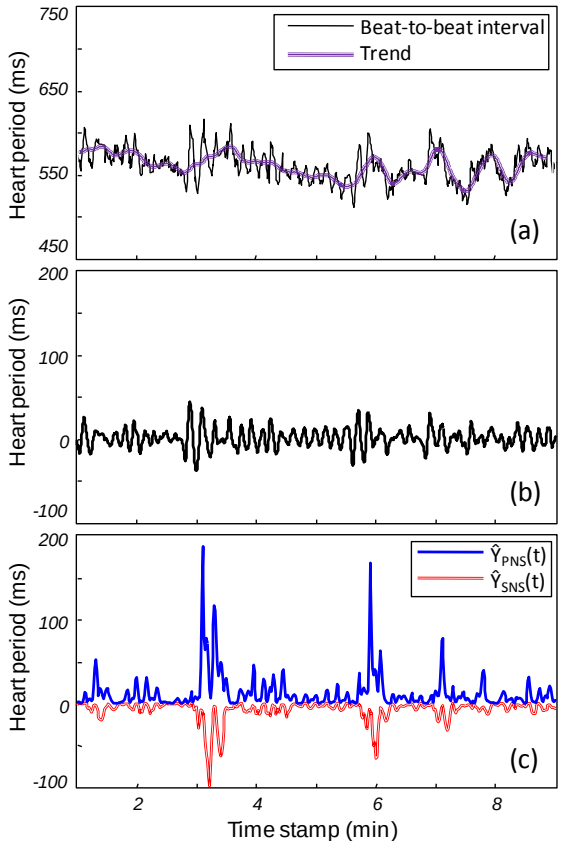

Figure 3. Signal processing steps. (a) Raw beat-to-beat signal and trend. (b) De-trended and band-pass filtered signal. (c) Positive and negative dynamics components from the PDM model

$y(t-1)$ as an input, and construct an initial PDM model: $\hat{Y}(t) = Y^T(t-1)QY(t-1)$. By construction, the residual error from this initial model ($x'(t) = y(t-1) - \hat{y}(t-1)$) will be broadband and will remain correlated with the output. We use this residual error as the final estimate of the input, and construct a final PDM model: $\hat{Y}(t) = X'^T(t)QX'(t)$.

4.2. Selecting principal dynamic modes

Once we have estimated the final PDM model, we must determine which of the different dynamic modes correspond to PNS activity, to SNS activity, and to noise. Zhong et al. [4] assigned the first two modes to PNS and SNS activity on the basis of their power spectral distribution, since one mode contained both LF and HF power, and the other mode contained mainly HF power. This assignment rule works well if the first two PDM eigenvalues have different sign. However, if the first two PDM eigenvalues have the same sign, their frequency content will not be predominantly LF (SNS-related) or LF-HF (PNS-related). Moreover, in the analysis of Zhong et al. [4] the first two PDMs capture over 90% of the system dynamics. In our experience, the first two PDM eigenvalues only capture about 60% of the dynamics in our data; additional modes are required to preserve a higher percentage of the dynamics.

To address these issues, we propose an alternative selection criterion. First, we discard any eigenvalues whose magnitude $|\lambda_i|$ is lower than 5% of the total energy $\sum|\lambda_i|$. Second, we assign negative eigenvalues to SNS activation, since both reduce heart periods (increase heart rate). Likewise, we assign positive eigenvalues to PNS activity, since both increase heart periods (decrease heart rate). Adding up positive and negative dynamics separately, we obtain the following estimates of PNS and SNS activity:

$$\hat{y}_{PNS}(t) = \sum_{\substack{\lambda_i>0 \\ |\lambda_i|/\sum|\lambda_k|>0.05}} \lambda_i\{pdm_i * X(t) + \mu_{i,0}\}^2 \quad (7)$$

$$\hat{y}_{SNS}(t) = \sum_{\substack{\lambda_i<0 \\ |\lambda_i|/\sum|\lambda_k|>0.05}} \lambda_i\{pdm_i * X(t) + \mu_{i,0}\}^2 \quad (7)$$

These assignments are more intuitive, and ensure that $\hat{y}_{PNS}(t)$ and $\hat{y}_{SNS}(t)$ capture a large percentage of the energy in the system's output (more than 90% in our data).

5. Methods

To validate the proposed method, we collected a dataset that consisted of heart-rate measurements from two experimental conditions: a tilt body posture and a supine body posture. In the tilt condition, the subject rested in an upright position at an angle of 70 degrees, whereas in the supine condition the subject lay in a horizontal position. These two conditions are standard in studies of cardiac regulation because they shift the autonomic balance: PNS is more dominant in a supine position, whereas SNS is more dominant in an upright position [2]. We performed eighteen experiments in the supine condition and twenty experiments in the tilt condition. Each experiment had a duration of nine minutes.

Heart period signals were sampled at a rate of 500 Hz, and processed with a peak-detection algorithm to identify the R waves [11]. The R-R period signal was then resampled at a rate of 4Hz via piecewise cubic Hermite interpolation. This instantaneous heart period was then processed with an aperiodic trend removal algorithm [12] and band-pass filtered between 0.04 Hz and 0.5 Hz to remove the VLF component. Finally, the signal was re-sampled at 1Hz for further analysis with

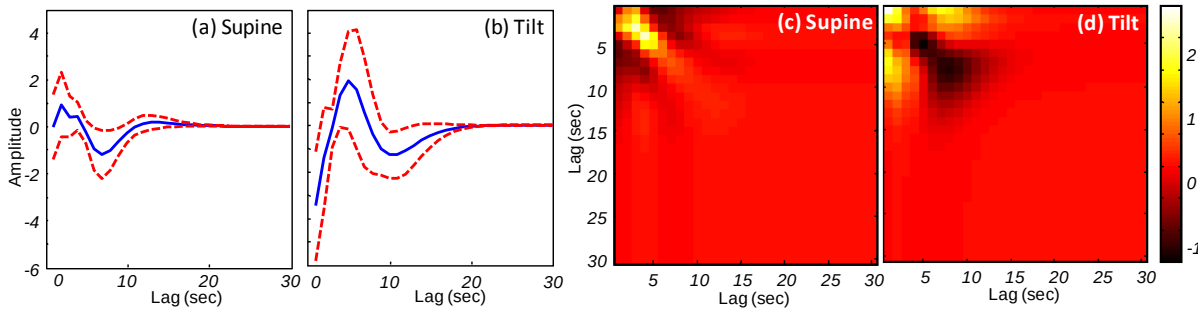

Figure 4. Volterra-Wiener kernel estimation with a memory of M = 30 seconds, Laguerre coefficient α = 0.2, and order L = 6 (refer to appendix). (a,b) First-order kernel for supine and tilt, averaged over the entire dataset; dashed line represents one standard deviation. (c,d) Second order kernel for supine and tilt. Notice how both conditions have different first and second-order dynamics.

the PDM and PSD methods. Results are shown in Figure 3(a,b).

For each experiment, the resulting signal was analyzed with a five-minute window, sliding at increments of 30-seconds. Thus, each nine-minute experiment resulted in seven frames. Each frame was treated as a sample, for a total of 126 supine samples and 140 tilt samples.

Separate PDM and PSD estimates were computed for each of these samples. Given that autonomic-state information is located in the 0.04-0.5Hz region, the PDM method used Volterra kernels with a memory of M=30 seconds. PSD estimates were obtained with Welch's method [13].

6. Results

Results from the Volterra kernel estimation are illustrated in Figure 4. First-order kernels $k_1(\tau)$ are consistent within experimental condition. Under the supine condition, $k_1(\tau)$ shows a predominantly positive influence from previous heart periods (4 seconds); this pattern is reversed for the tilt condition. In both cases, linear influences from previous samples die out after 20 seconds, which indicates that the kernel memory (30 seconds) is appropriate. The second-order kernel $k_2(\tau_1, \tau_2)$ for the supine condition shows positive coefficients between close terms (main diagonal block), and negative coefficients for other terms (diagonal bands). In contrast, $k_2(\tau_1, \tau_2)$ for the tilt condition contains positive coefficients between close terms (diagonal bands), and negative coefficients for other terms (main diagonal block). These results suggest that the two physiological conditions may be discriminated based on their dynamics.

6.1. Principal dynamic analysis

Results from the PDM analysis are illustrated in Figure 5 for a 5-minute sample from each experimental condition. For the supine condition (Figure 5 (a)), three of the five significant eigenvalues are positive, and their sum is larger than the sum of negative eigenvalues (i.e., $\sum|\lambda_i^+| > \sum|\lambda_i^-|$). For the tilt condition, in contrast, the sum of negative eigenvalues is larger than the sum of positive eigenvalues (Figure 5(b)). The power spectral density of PNS components and SNS components is shown in Figure 5 (c,d); their time-domain signals are shown in Figure 3(c). Activation of the PNS component is higher for the supine condition than for the tilt condition, whereas the opposite is true for the SNS component. Moreover, the PNS component tends to have a broad distribution of energy across LF and HF bands, whereas the SNS component is more dominant in the LF region; these results are consistent with the frequency characteristics of each branch. For comparison purposes, Figure 5 (c,d) also shows the PSD of the original signal $y(t)$; in both conditions, the spectral power concentrates on the LF region, and the LF/HF ratio remains similar for both conditions. This result illustrates the shortcomings of traditional spectral analysis based on the LF/HF ratio.

6.2. Classification performance

We also compared PSD analysis and the PDM method in terms of classification performance. For this purpose, we extracted two features from the PSD (spectral power in the LF and HF bands) and six features from the PDM (sum of significant eigenvalues, and spectral power in LF and HF bands for $\hat{y}_{PNS}(t)$ and $\hat{y}_{SNS}(t)$).

Classification performance was measured with a k=7 nearest neighbor rule operating in the Fisher's linear discriminant analysis (LDA) projection computed on training data[4]. Each classification run was

[4] For binary discrimination problems, Fisher's LDA reduces to a single projection axis.

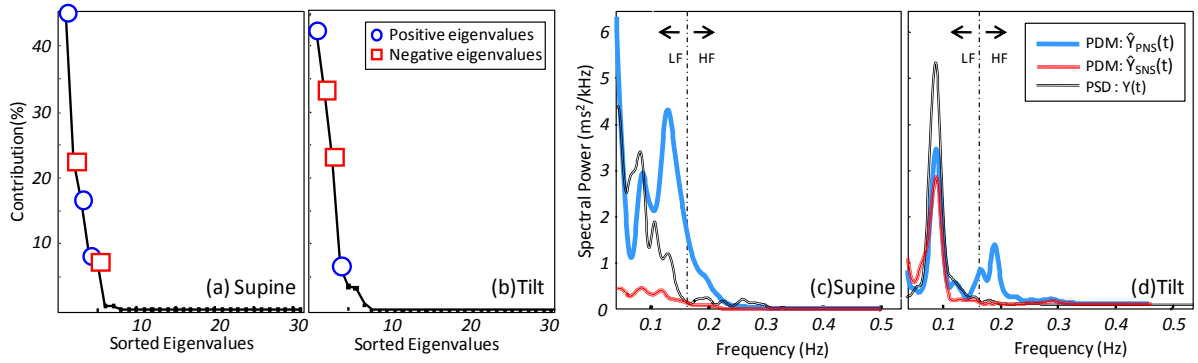

Figure 5. Magnitude of eigenvalues for (a) supine and (b) tilt. Power spectra of $\hat{y}_{PNS}(t)$, $\hat{y}_{SNS}(t)$, and $y(t)$ for (c) supine and (d) tilt.

repeated 1,000 times with two forms of random subsampling: experiment-wise and sample-wise. In the case of experiment-wise partitions, all the samples from 5 randomly-chosen experiments out of 38 experiments were used for testing, and samples from the remaining experiments were used for training. In the case of sample-wise partitions, 50 randomly-chosen samples out of 266 samples (38 experiments $\times$ 7 samples) were used for testing and the remaining samples were used for training. Experiment-wise partitioning is a more realistic validation procedure, since samples from a particular experiment are classified based on samples from other experiments. In contrast, sample-wise partitioning allows samples from a particular experiment to appear both in the training set and in the test set, which can lead to overly optimistic results. Thus, classification rates on these two validation procedures serve as lower and upper bounds, respectively.

Classification results are summarized in Figure 6. PDM provides higher classification rate on both validation procedures. This improvement in performance can be attributed to the fact that the PDM method separates the dynamics of the two autonomic branches, which cannot be done with the PSD since the LF component is influenced by both branches, as was illustrated in Figure 5 (c,d).

6.3. Interpolation capabilities

The supine and tilt conditions are just two out of many potential autonomic states. How well does the PDM method generalize to different states? To answer this question, we performed an additional set of experiments under a 60-degree tilt condition. Our expectation was that this intermediate position would map between the 70°-tilt and the supine postures. Figure 7 shows the projection of 60°-tilt samples onto the LDA eigenvector defined by the supine and 70°-tilt conditions. For the PSD method, 60°-tilt samples are confounded with the 70°-tilt samples, whereas in the PDM method they map between the supine and 70°-tilt conditions. These results indicate that the PDM method provides a more fine-grained and monotonic discrimination between physiological conditions. This result is important when considering our ultimate goal: being able to cluster the physiological state of a user under naturalistic conditions, where autonomic state may be described more as a continuum than as a set of discrete states.

7. Conclusion

We have presented a computational method to estimate sympathetic (stress-related) and parasympathetic (relaxation-related) activation from a consumer-grade heart rate monitor (HRM). Our approach is based on the principal dynamic modes of Marmarelis [6, 7], later revised by Zhong et al. [4, 5] for the analysis of heart rate variability from ECG recordings. Our contribution to this prior work is three-fold. First, we have shown that the PDM model can be used to estimate autonomic activation using HRMs commonly used for exercise management. This result is significant because HRMs are low-cost (one to two orders of magnitude lower than ambulatory ECG monitors) and considerably less unobtrusive. Second, our results show that the PDM model can be used to discriminate physiological states induced without pharmacological blockade. This result is significant because it may enable the use of the PDM methodology on ecological scenarios, i.e., experience sampling as the user goes through her day. Third, we have proposed an alternative selection criterion for principal dynamic modes. Namely, our approach considers positive and negative "eigen-dynamics" as indices of parasympathetic and sympathetic activation, respectively. This criterion is superior to that proposed by Zhong et al. [4] because it assigns eigenvectors based on their polarity rather than their frequency

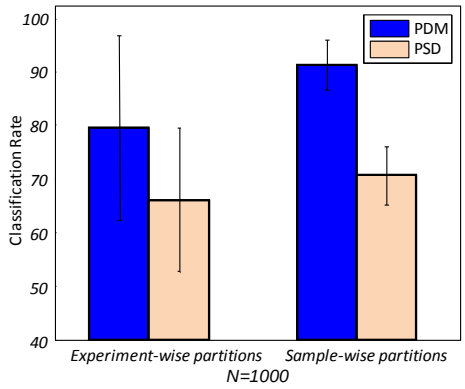

Figure 7. Recognition rate for experiment-wise and sample-wise validation

content. The PDM method also shows higher discrimination performance than traditional power spectral analysis of heart rate variability. The merit of the approach lies in its ability to separate cardiac dynamics in a manner that is consistent with autonomic regulation.

Autonomic state is commonly regarded as a one-dimensional continuum, where sympathetic and parasympathetic branches are under reciprocal control, e.g., when one increases, the other decreases. However, it has been shown that reciprocity is just one of several modes of autonomic control: coactivation and uncoupled activation are also possible [14]. Thus, autonomic state is better described as a two-dimensional continuum [1]. More recently, Backs [15] has shown that these different modes of autonomic control (e.g., reciprocity, coactivity, and uncoupled control of either branch) map onto mental-workload states in a context-dependent one-to-one fashion, i.e., what Cacioppo and Tassinary [16] defined as a psychophysiological marker. By combining this finding with the separate prediction of sympathetic and parasympathetic activation we have presented, the mapping from raw physiological data onto psychological processes may then become straightforward. This methodology stands in contrast to ad-hoc approaches that rely on pattern-recognition techniques to find a mapping from physiological to psychological state.

The PDM approach may afford greater insight to life styles when combined with context data, e.g., from location or ambient sensors. In particular, the better generalization properties of the PDM method suggest that it could provide a more meaningful clustering of daily living events, which would ultimately afford better cues to the user's life patterns, e.g., patterns of stress or mental load through the day. As a result, estimates of autonomic balance may not only help identify habits but could also provide objective

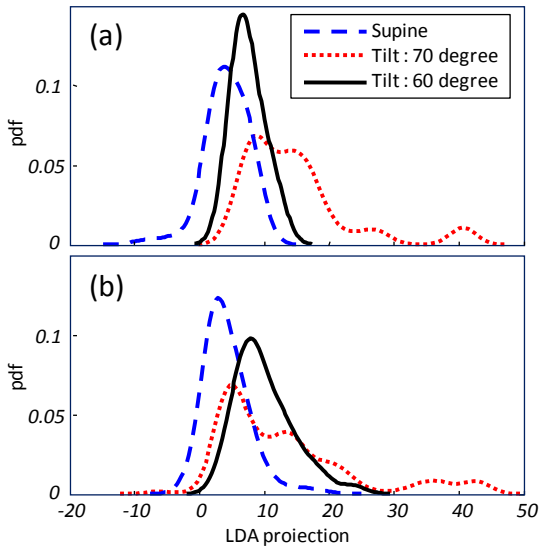

Figure 6. Parzen density estimate of the LDA projection with supine, 70°-tilt, and 60°-tilt using (a) PDM and (b) PSD

feedback to users interested in developing healthier behaviors.

Appendix: Estimating Volterra kernels

Estimation of the Volterra kernels is a challenging computational problem due to the correlation between the basis functions $x^k(t)$. Several methods (e.g., cross-correlation, fast orthogonal, differential sampling) are available to estimate Volterra kernels, but Wiener's method [17] is known to yield accurate low-order kernel estimates from short experimental data recordings, even in the presence of considerable noise [6]. The key element of this method is the assumption that the Volterra kernels have a block structure, in which the input x(t) is first passed through a filter bank $\{b_k(\tau); k = 0 \dots L-1\}$:

$$v_j(t) = \sum_{\tau=0}^{M-1} b_k(\tau) x(t-\tau) \qquad (8)$$

and the corresponding outputs $v_j(t)$ are then combined through a static nonlinearity:

$$y(t) = f\big(v_1(t), v_2(t), \dots, v_j(t), \dots\big) \qquad (9)$$

By making this assumption, the Volterra series in equation (1) become a multinomial expansion[5]:

[5] Note that the time lag τ has been eliminated from the filter-bank outputs $v_j(t)$ and has been absorbed by the expansion coefficients

$$y(t) = c_0 + \sum_{j=0}^{L-1} c_1(j) v_j(t) + \sum_{j_1=0}^{L-1} \sum_{j_2=0}^{L-1} c_2(j_1, j_2) v_{j_1}(t)\, v_{j_2}(t) + \cdots \quad (10)$$

from which the unknown expansion coefficients can be estimated via time-averaging of covariance samples [17]:

$$c_0 = E[y]$$
$$c_1(j) = \frac{1}{A} E\left[y * v_j\right] \quad (11)$$
$$c_2(j_1, j_2) = \frac{1}{2A^2} E\left[y * \{v_{j_1} * v_{j_2} - A\delta_{j_1, j_2}\}\right]$$

where A is the input power, and δ is the Dirac delta function. As a result, matrix Q in equation (2) can be constructed from the estimated multinomial kernels as:

$$Q = \begin{bmatrix} c_0 & \frac{1}{2} {c_1}^T B^T \\ \frac{1}{2} B c_1 & B^T c_2 B \end{bmatrix} \quad (12)$$
$$where\ B = \begin{bmatrix} {b_0}^T & {b_1}^T & \dots & {b_{L-1}}^T \end{bmatrix}$$
$$and\ b_k = [b_k(0) \quad b_k(1) \quad \dots \quad b_k(M-1)]$$

As suggested by Wiener, a suitable orthonormal basis for the impulse responses $\{b_k(\tau)\}$ in equation (8) is the family of Laguerre polynomials. These functions behave as exponential decays, which makes them particularly well suited for modeling physiological systems. Laguerre functions are defined as:

$$b_k(\tau) = \alpha^{(\tau-k)/2}(1-\alpha)^{1/2} \times \sum_{i=0}^{k} (-1)^i \binom{\tau}{i} \binom{k}{i} \alpha^{k-i}(1-\alpha)^i \quad (13)$$

where $k = 0, \dots, L-1$ is the order of the Laguerre function, $\tau = 0, \dots, M-1$ is the number of lags, and α is the Laguerre coefficient. Values of α=0.2 and L=6 were used in this work. A value of α=0.2 ensures that the Laguerre functions die out within the 30-sec lag of the Volterra kernel.

References

[1] J. T. Cacioppo, L. G. Tassinary, and G. Berntson, Handbook of Psychophysiology 3ed.: Cambridge University Press, 2007.

[2] M. Malik, A. J. Camm, J. J. Thomas Bigger et al., "Heart rate variability: standards of measurement, physiological interpretation and clinical use," Circulation, vol. 93, no. 5, pp. 1043-65, March 1, 1996.

[3] T. E. Brown, L. A. Beightol, J. Koh et al., "Important influence of respiration on human R-R interval power spectra is largely ignored," Journal of Applied Physiology, vol. 75, no. 5, 1993.

[4] Y. Zhong, H. Wang, K. H. Ju et al., "Nonlinear analysis of the separate contributions of autonomic nervous systems to heart rate variability using principal dynamic modes," IEEE Transactions on Biomedical Engineering, vol. 51, no. 2, pp. 255-262, Feb. , 2004.

[5] Y. Zhong, K.-M. Jan, K. H. Ju et al., "Quantifying cardiac sympathetic and parasympathetic nervous activities using principal dynamic modes analysis of heart rate variability," American Journal of Physiology(AJP) - Heart and Circulatory Physiology, vol. 291, no. 3, pp. H1475–H1483, April 7, 2006.

[6] V. Z. Marmarelis, "Identification of nonlinear biological systems using laguerre expansions of kernels " Annals of Biomedical Engineering, vol. 21, no. 6, pp. 573-589, November, 1993.

[7] V. Z. Marmarelis, "Modeling Methodology for Nonlinear Physiological Systems," Annals of Biomedical Engineering, vol. 25, pp. 239-251, 1997.

[8] R. Jain, "Experiential computing," Communications of the ACM vol. 46, no. 7, pp. 48-55, July, 2003.

[9] M. Radespiel-Tröger, R. Rauh, C. Mahlke et al., "Agreement of two different methods for measurement of heart rate variability," Clinical Autonomic Research, vol. 13, no. 2, pp. 99-102, 2003 Apr, 2003.

[10] R. Moll. "HRM Receiver Board "; http://rick.mollprojects.com/hrm/index.html. 2005.

[11] G. M. Friesen, T. C. Jannett, M. A. Jadallah et al., "A comparison of the noise sensitivity of nine QRS detection algorithms," IEEE Transactions on Biomedical Engineering, vol. 37, no. 1, pp. 85-98, 1990.

[12] M. P. Tarvainen, P. O. Ranta-aho, and P. A. Karjalainen, "An advanced detrending method with application to HRV analysis," IEEE Transactions on Biomedical Engineering, vol. 49, no. 2, pp. 172-175, 2002.

[13] P. D. Welch, "The use of fast Fourier transform for the estimation of power spectra: A method based on time averaging over short, modified periodograms," IEEE Transactions of Audio and Electroacoustics, vol. 15, no. 2, pp. 70-73, 1967.

[14] R. W. Backs, "An autonomic space approach to the psychophysiological assessment of mental workload," Stress, Workload, and Fatigue Human Factors in Transportation: Lawrence Erlbaum Associates, 2001.

[15] R. W. Backs, "An autonomic space approach to the psychophysiological assessment of mental workload," Stress, Workload, and Fatigue, P. A. Hancock and P. A. Desmond, eds., pp. 279-289, 2001.

[16] J. T. Cacioppo, and L. G. Tassinary, "Inferring psychological significance from physiological signals," American Psychologist, vol. 45, no. 1, pp. 16-28, 1990, 1990.

[17] N. Wiener, Nonlinear problems in random theory, Cambridge: Technology Press of Massachusetts Institute of Technology, 1958.